Delft University of Technology

Directional Total Variation Regularized High-Resolution Prestack AVA Inversion

Huang, Guangtan; Chen, Xiaohong; Qu, Shan; Bai, Min; Chen, Yangkang

Citation (APA)
Huang, G., Chen, X., Qu, S., Bai, M., & Chen, Y. (2021). Directional Total Variation Regularized High-Resolution Prestack AVA Inversion. *IEEE Transactions on Geoscience and Remote Sensing*, *60*. https://doi.org/10.1109/TGRS.2021.3078293

Important note
To cite this publication, please use the final published version (if applicable).
Please check the document version above.

This article has been accepted for inclusion in a future issue of this journal. Content is final as presented, with the exception of pagination.

IEEE TRANSACTIONS ON GEOSCIENCE AND REMOTE SENSING   1

Directional Total Variation Regularized High-Resolution Prestack AVA Inversion

Guangtan Huang[ID], Xiaohong Chen[ID], Shan Qu, Min Bai[ID], and Yangkang Chen[ID], *Member, IEEE*

Abstract—Prestack seismic inversion has emerged as a powerful technique for reconstructing parameters attribute to the subsurface properties and building the geophysical parameter models. However, the inversion algorithms always suffer from spatial blur and low resolution. Total variation (TV) regularization preserves the spatial variation boundary of data by highlighting the sparsity of the first-order difference, which is regarded as an important technical means for image restoration. However, when the data do not change along the spatial grid direction, TV regularization is prone to a staircase effect. In this article, a directional TV (DTV) method is proposed to conduct the prestack amplitude variation with offset/angle (AVO/AVA) inversion. The method consists of three essential steps: estimating the seismic slope attribute from the seismic data, introducing seismic slope attribute to the TV regularization to establish the objective function, and optimizing the objective function by the split-Bregman algorithm. Finally, the conventional and proposed methods are applied to the synthetic and the real seismic data. The comparison of different methods demonstrates that the proposed method is applicable to reveal the detailed subsurface models, alleviate the staircase effect or artifact substantially, and further upgrade the quality of prestack inversion results.

Index Terms—Directional total variation (DTV), high resolution, prestack amplitude variation with angle (AVA) inversion, seismic slope.

I. Introduction

PRESTACK amplitude variation with offset/angle (AVO/AVA) inversion quantitively extracts rock elastic parameters regarding the subsurface properties, which has been proven to be of significance for exploration geophysics [1]–[5]. Although sustained efforts have been made in both theoretical and engineering applications to improve the

accuracy, resolution, and robustness of the inversion results [6]–[11], there are still many problems. The realization process can be regarded as minimizing the error between the observed seismic data and the synthetic data under the premise of certain geological and geophysical data constraints.

Due to the convolutional effect of the seismic wavelet, which leads to the degradation of the ability to characterize the structure and lithology of subsurface media, it is difficult to perform a detailed interpretation of the seismic inversion. Besides, another reason that causes the low resolution is the smoothness constrained regularization. By imposing additional constraints of the prior information or knowledge on the estimated models, the Tikhonovo-type-based regularizations are often adopted to mitigate the ill-posedness induced by various reasons, such as noise and inappropriate forward operator. Especially, if the Zoeppritz equation [12], [13] is exploited as a forward operator to directly invert V_p, V_s, and ρ, the Gaussian distribution (corresponding to the ℓ_2-norm) is usually selected as the constraint. Such constraints will greatly limit the resolution of the inversion results because the ℓ_2-norm is a smooth constraint, resulting in the defects of blurred reflection interfaces and insufficient ability to describe special geological structures [14]–[16]. In addition, the traditional prestack AVA inversion is based on the angle gather data to invert the single trace data [17]–[22]. Throughout the inversion process, it always relatively uses a single trace, which does not fully make use of the horizontal constraints. Due to the lack of constraints in the lateral direction of the inversion results, it sometimes causes poor lateral resolution and continuity. Therefore, to incorporate *a priori* knowledge into seismic inversion, both the stability and resolution (in both horizontal and vertical direction) should be taken into account [23]–[28]. At present, most prestack inversion algorithms are based on single prestack angle gathers. Such algorithms do not take into account adjacent data, and the inversion process of each trace is relatively independent.

To improve the vertical resolution of the inversion, some sparse distributions are introduced as *a priori* information for the seismic inversion. Alimie and Sacchi [29] introduced the trivariation Cauchy regularization to the seismic inversion. Zhang and Castagna [30] introduced basis-pursuit inversion (BPI), which is a ℓ_1-norm regularized optimization algorithm, into seismic reflection inversion. Then, Zhang et.al. [31] applied BPI to the prestack AVA inversion and simultaneously obtain multiple reflectivity series $\mathbf{r}_{vp}$, $\mathbf{r}_{vs}$, and $\mathbf{r}_\rho$.
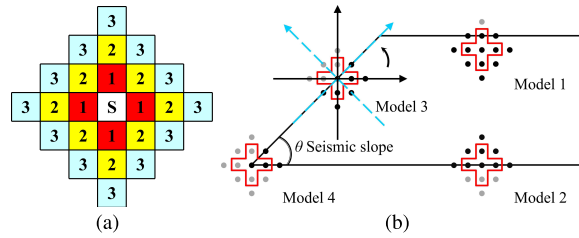
Fig. 1. (a) TV regularization for a spatial point S with first-, second-, and third-order differences using the correspondingly labeled points and (b) schematic illustration of geological structure with the models (spatial points) for the first-order difference TV regularization (within the red lines). Note that Model 1 corresponds to the points located at the isotropic media; Models 2 indicates the points located at the horizontal interface; Model 3 denotes the points located at the tilted boundary; and Model 4 represents the points located at the vanishing point of special geological body.

In image processing, the total variation (TV) regularization [or the Markov random field (MRF)] is usually adopted as a constraint to solve the inverse problems, which is an effective spatial texture modeling tool [7], [32]–[37]. Anagaw and Sacchi [38] introduced the TV regularization to the impedance inversion. Gholami [39] proposed a multitrace impedance inversion method with 2-D TV regularization to make sure that the inversion results follow the spatial and temporal correlations of the seismic data. TV regularization describes the spatial variation boundary of data by highlighting the sparsity of the first-order difference, which is regarded as an important technical means for image restoration. However, different from the digital images, the subsurface properties always change according to some specific geologic structures, such as the tilted layers, faults, and edges of some special geological bodies. Regardless of the geologic direction of the subsurface medium, the TV regularization only tends to reduce the horizontal and vertical gradients of each grid point in the model. Once the data do not change along the spatial grid direction, TV regularization is prone to a staircase effect. It is mainly reflected in the insufficient ability to describe faults, titled strata with a large slope, and some special rock bodies. Therefore, TV is not suitable for the stratum where the local structure has a dominant direction [40], [41]. The MRF scheme [7] takes into account diagonal directions within the neighborhood system. As shown in Fig. 1(a), TV or high-order TV regularization can only take the points along the horizontal and vertical axes, while MRF can take the points in the diagonal directions into account.

Indeed, the conventional inversion is comprehensive for the utilization of seismic data, especially for the usage of long-wavelength components of seismic data. The travel time information in seismic data usually corresponds to the long-wavelength component [42]–[48], which is often related to tectonic information, while the amplitude and waveform information usually corresponds to the mid-short wavelength component, which is often related to lithological information [49]. At present, the prestack AVA inversion mainly focuses on amplitude information, but the long-wavelength components related to structural information have not enough attention. Here, we introduce the seismic slope attribute, a kind

of structure information, to the TV regularization algorithm, so as to improve the application effect of the TV regularization method.

The seismic slope attribute can be extracted using the plane wave destruction (PWD) technique [50]–[53], which indicates the seismic event slope and is one of the seismic attributes related to the seismic long-wavelength component. Indeed, it is also a good lateral constraint condition, which has been widely used in the data regularization [54], [55] and full-waveform inversion [56], [57] based on the shaping regularization.

This article is organized as follows. First, the prestack AVA inversion based on the exact Zoeppritz equation and the seismic slope attribute extraction based on the PWD are first briefly reviewed. Then, the proposed directional TV (DTV) regularization based on the seismic slope attribute is introduced into the seismic inversion. Finally, the proposed method is demonstrated by the synthetic data and further validated by the real seismic data.

II. THEORY

A. Exact Zoeppritz Equation Inversion

According to the Zoeppritz's equation, the reflection and transmission coefficients can be expressed as

$$\mathbf{Ar} = \mathbf{b} \tag{1}$$

where $\mathbf{A}$ and $\mathbf{b}$ are the coefficient matrices composed of the elastic parameters V_{p1}, V_{p2}, V_{s1}, V_{s2}, ρ_1, and ρ_2 of the upper and lower media and the angle-dependent parameters, and $\mathbf{r}$ is the reflection and transmission coefficient vector. Their explicit formulas are expressed as (5).

Then, the P-P seismic data can be simulated by convolving the P-P reflectivity coefficient with the stationary wavelet as

$$\mathbf{d} = \mathbf{Wr(m)} \tag{2}$$

or

$$\mathbf{d} = \mathbf{G(m)} \tag{3}$$

and the partial derivative with respect to the parameter $\mathbf{m}$ can be expressed as

$$\frac{\partial \mathbf{r}}{\partial \mathbf{m}} = \mathbf{A}^{-1} \left(\frac{\partial \mathbf{b}}{\partial \mathbf{m}} - \frac{\partial \mathbf{A}}{\partial \mathbf{m}} \mathbf{r} \right) \tag{4}$$

where the expressions of the $(\partial \mathbf{A}/\partial \mathbf{m})$ and $(\partial \mathbf{b}/\partial \mathbf{m})$ are detailed in (5)–(11), as shown at the bottom of the next page.

B. Seismic Local Slope Attribtue Extraction

The seismic local slope attribute is a widely used tool in exploration geophysics [51]. Its applications include wavefield separation, denoising, seislet transform, predictive painting, and so on. According to Claerbout [50], the plane wave can be expressed by the first-order differential equation as follows:

$$\frac{\partial P(x,t)}{\partial x} + \sigma(x,t)\frac{\partial P(x,t)}{\partial t} = 0 \tag{12}$$

This article has been accepted for inclusion in a future issue of this journal. Content is final as presented, with the exception of pagination.

HUANG *et al.*: DTV REGULARIZED HIGH-RESOLUTION PRESTACK AVA INVERSION

3

where $P(x, t)$ represents the plane wavefield, and $\sigma(x, t)$ indicates the local slope. In the discrete space, the slope between the adjacent points (spatial interval Δx) can be expressed by the time interval Δt and $\sigma(x, t)$

$$p = \sigma(x, t) \Delta x / \Delta t. \tag{13}$$

In the local scope, the wavefield value is consistent; then

$$P(x, t) = P(x + \Delta x, t + p \Delta t). \tag{14}$$

Transforming (14) from the $X - T$ domain to the $Z_x - Z_t$ domain using the Z transform, the above equation becomes

$$(1 - Z_x Z_t^p) P(Z_x, Z_t) = 0 \tag{15}$$

where Z_x and Z_x represent the spatial- and time-shift operators. Here, $C(p) = (1 - Z_x Z_t^p)$ is the so-called plane-wave

destruction operator. By using Thiran's fractional delay filter $(1/B(Z_t)/B(Z_t))$ to approximate the time-shift operator $e^{i\omega\sigma}$ [58], the plane-wave destructor can be rewritten as

$$C(p, Z_t, Z_x) = B(Z_t) - Z_x B\left(\frac{1}{Z_t}\right), \quad B(Z_t) = \sum_{n=-N}^{N} b_k Z_t^{-k}. \tag{16}$$

The coefficient of filter $B(Z_t)$ can be obtained by fitting the filter frequency response at low frequencies to the response of the phase shift operator. We can determine the slope by minimizing the following least-squares goal based on using an iterative method, such as Newton's method:

$$C(\sigma, Z_x, Z_t) P(Z_x, Z_t) \approx 0. \tag{17}$$

$$\frac{\partial \mathbf{A}}{\partial V_{p1}} = \frac{1}{V_{p1}} \cdot \begin{bmatrix} 0 & \tan\phi \sin\phi_1 & \sin\theta_2 & \tan\phi_2 \sin\phi_2 \\ 0 & \sin\phi_1 & \sin\theta_2 \tan\theta_2 & -\sin\phi_2 \\ 2(1 - \cos 2\phi_1) & (2 - \tan^2\phi_1)\dfrac{V_{s1}}{V_{p1}}\sin 2\phi_1 & \dfrac{\rho_2}{\rho_1}\dfrac{V_{p2}}{V_{p1}}(3\cos 2\phi_2 - 2) & (2 - \tan^2\phi_2)\dfrac{\rho_2}{\rho_1}\dfrac{V_{s2}}{V_{p1}\sin 2\phi_2} \\ 0 & \dfrac{V_{p1}}{V_{s1}}(2 - \cos 2\phi_1) & \dfrac{\rho_2}{\rho_1}\dfrac{V_{s2}^2}{V_{s1}^2}\dfrac{V_{p1}}{V_{p2}}\sin 2\theta_2 \tan^2\theta_2 & \dfrac{\rho_2 V_{p1} V_{s2}}{\rho_1 V_{s1}^2}(\cos 2\phi_2 - 2) \end{bmatrix} \tag{5}$$

$$\frac{\partial \mathbf{A}}{\partial V_{s1}} = \frac{1}{V_{s1}} \begin{bmatrix} 0 & -\tan\phi_1 \sin\phi_1 & 0 & 0 \\ 0 & -\sin\phi_1 & 0 & 0 \\ 4\sin^2\phi_1 & (\tan^2\phi_1 - 2)\dfrac{V_{s1}}{V_{p1}}\sin 2\phi_1 & 0 & 0 \\ 0 & \dfrac{V_{p1}}{V_{s1}}(\cos 2\phi_1 - 2) & -2\dfrac{\rho_2 V_{s2}^2 V_{p1}}{\rho_1 V_{s1}^2 V_{p2}}\sin 2\theta_2 & 2\dfrac{\rho_2}{\rho_1}\dfrac{V_{s2} V_{p1}}{V_{s1}^2}\cos 2\phi_2 \end{bmatrix} \tag{6}$$

$$\frac{\partial \mathbf{A}}{\partial \rho_1} = \frac{1}{\rho_1} \begin{bmatrix} 0 & 0 & 0 & 0 \\ 0 & 0 & 0 & 0 \\ 0 & 0 & \dfrac{\rho_2}{\rho_1}\dfrac{V_{p2}}{V_{p1}}\cos 2\phi_2 & \dfrac{\rho_2}{\rho_1}\dfrac{V_{s2}}{V_{p1}}\sin 2\phi_2 \\ 0 & 0 & -\dfrac{\rho_2}{\rho_1}\dfrac{V_{s2}^2}{V_{s1}^2}\dfrac{V_{p2}}{V_{p1}}\sin 2\theta_2 & \dfrac{\rho_2}{\rho_1}\dfrac{V_{s2} V_{p1}}{V_{s1}^2}\cos 2\phi_2 \end{bmatrix} \tag{7}$$

$$\frac{\partial \mathbf{A}}{\partial V_{p2}} = \frac{1}{V_{p2}} \begin{bmatrix} 0 & 0 & -\sin\theta_2 & 0 \\ 0 & 0 & -\sin\theta_2 \tan\theta_2 & 0 \\ 0 & 0 & -\dfrac{\rho_2}{\rho_1}\dfrac{V_{p2}}{V_{p1}}\cos 2\phi_2 & 0 \\ 0 & 0 & -\dfrac{\rho_2}{\rho_1}\dfrac{V_{s2}^2}{V_{s1}^2}\dfrac{V_{p1}}{V_{p2}}\sin 2\theta_2 \tan^2\theta_2 & 0 \end{bmatrix} \tag{8}$$

$$\frac{\partial \mathbf{A}}{\partial V_{s2}} = \frac{1}{V_{s2}} \begin{bmatrix} 0 & 0 & 0 & -\tan\phi_2 \sin\phi_2 \\ 0 & 0 & 0 & \sin\phi_2 \\ 0 & 0 & 2\dfrac{\rho_2}{\rho_1}\dfrac{V_{p2}}{V_{p1}}(1 - \cos 2\phi_2) & \dfrac{\rho_2}{\rho_1}\dfrac{V_{s2}}{V_{p1}}\sin 2\phi_2(2\tan^2\phi_2 - 2) \\ 0 & 0 & \dfrac{\rho_2}{\rho_1}\dfrac{V_{s2}^2}{V_{s1}^2}\dfrac{V_{p1}}{V_{p2}}\sin 2\theta_2 & -\dfrac{\rho_2}{\rho_1}\dfrac{V_{p1} V_{s2}}{V_{s1}^2}(2 + 3\cos\phi_2) \end{bmatrix} \tag{9}$$

$$\frac{\partial \mathbf{A}}{\partial \rho_1} = \frac{1}{\rho_2} \begin{bmatrix} 0 & 0 & 0 & 0 \\ 0 & 0 & 0 & 0 \\ 0 & 0 & -\dfrac{\rho_2}{\rho_1}\dfrac{V_{p2}}{V_{p1}}\cos 2\phi_2 & -\dfrac{\rho_2}{\rho_1}\dfrac{V_{s2}}{V_{p1}}\sin 2\phi_2 \\ 0 & 0 & \dfrac{\rho_2}{\rho_1}\dfrac{V_{s2}^2}{V_{s1}^2}\dfrac{V_{p2}}{V_{p1}}\sin 2\theta_2 & -\dfrac{\rho_2}{\rho_1}\dfrac{V_{s2} V_{p1}}{V_{s1}^2}\cos 2\phi_2 \end{bmatrix} \tag{10}$$

$$\frac{\partial \mathbf{B}}{\partial V_{p1}} = \frac{1}{V_{p1}}\begin{bmatrix} 0 & 0 & -4\sin^2\phi_1 & 0 \end{bmatrix}^T, \quad \frac{\partial \mathbf{B}}{\partial V_{p2}} = \frac{\partial \mathbf{B}}{\partial V_{s1}} = \frac{\partial \mathbf{B}}{\partial V_{s2}} = \frac{\partial \mathbf{B}}{\partial \rho_1} = \frac{\partial \mathbf{B}}{\partial \rho_2} = \begin{bmatrix} 0 & 0 & 0 & 0 \end{bmatrix}^T \tag{11}$$

C. Automatic Directional Total Variation Constraint

In addition to structural information, the exploration and development process pays more attention to the fluid information in the reservoir. The information related to the physical characteristics of the reservoir (such as Poisson's ratio, V_p/V_s, and density ρ) often exists in the middle and far angle data. Therefore, the seismic prestack mid- and far-angle data should be more effective in the seismic prestack inversion, and the accuracy of the forward operator simulation is improved, especially in the mid- and far-angle accuracies. Furthermore, improving the accuracy of physical property information estimation is crucial for oil/gas exploration and development. Thus, the forward problem can be expressed as

$$0 = F(\mathbf{d}, \mathbf{m}) = \mathbf{d} - G(\mathbf{m}) \tag{18}$$

where $\mathbf{m}$ indicates the elastic parameters $[V_p, V_s, \rho]$, $\mathbf{d}$ represents observed seismic data, and G is the nonlinear forward operator, which is a function of model parameters. In practical applications, solving the inverse problem of (18) is usually ill-posed, and the inverse problem needs to be solved using the regularization method. According to the Bayesian theory, the objective function can be expressed as

$$J(\mathbf{m}) = ||\mathbf{d} - G(\mathbf{m})||_2^2 + \lambda Rc(\mathbf{m}) \tag{19}$$

where λ denotes the tradeoff factor, which balances the noise and model regularization. $||\mathbf{d} - G(\mathbf{m})||$ corresponds to the likelihood function, and $Rc(\mathbf{m})$ represents the prior distribution, which is also called a penalty norm, e.g., a function of model $\mathbf{m}$. The prior distribution explains the distribution of the target parameters.

Generally, the elastic parameters $[V_p, V_s, \rho]^T$ are assumed to obey the Gaussian distribution. However, such an assumption would lead to oversmooth results. Such inversion results have poor ability to describe the internal details of the reservoir and the boundary of the reservoir.

We consider anisotropic TV as the basic regularization method because the TV can smooth the model and, at the same time, preserve edges by enhancing the sparsity of the spatial gradient of the velocity difference. In addition, the anisotropic version is easier to minimize compared with the isotropic one. Furthermore, we restrict ourselves to the 2-D case although an extension to the full 3-D situation is relatively straightforward.

The extended misfit function with a TV constraint can be expressed as

$$J_{\text{tv}}(\mathbf{m}) = J(\mathbf{m}) + \alpha(||\nabla_x \mathbf{m}||_1 + ||\nabla_z \mathbf{m}||_1) \tag{20}$$

where ∇_x and ∇_z denote the horizontal- and vertical-gradient operators in a Cartesian coordinate, which can be expressed as

$$\nabla_x \mathbf{m}(i, j) = \mathbf{m}_{i+1,j} - \mathbf{m}_{i,j}, \nabla_z \mathbf{m}(i, j) = \mathbf{m}_{i,j+1} - \mathbf{m}_{i,j}. \tag{21}$$

The horizontal and vertical gradients are the spatial finite differences of the model, which is also called an MRF. In the optimization, more points can be introduced to participate in the difference operations to relieve the influence of abnormality of individual points. Due to $(2k + 1)$ points involved in the difference calculation, it is also called a k-order MRF, as shown in Fig. 1(a). Thus, (19) corresponds to the first-order MRF.

However, traditional TV regularization can only regularize the model in the horizontal and vertical directions regardless of the geological structure. Thus, the target parameters with severe lateral tectonic fluctuations, such as tilted layers, faults, and salt body, are not appropriate to apply the conventional TV regularization. However, the x- and z-directions can be rotated following the directions perpendicular or normal to the dip direction.

Fig. 1(b) shows the stratum at a fault, and we use the four position points as the model corresponding to models 1–4. The red boxes indicate the points involved in the operation of the first-order difference. Model 1 denotes the points within the stratum, which can get good results using traditional inversion algorithms. Model 2 represents the point located at the horizontal stratum interface. In order to clearly depict the information at this point, using the traditional TV regularization can yield the results with ideal effect. Model 3 corresponds to the point at the tilted fault, which cannot describe the fault interface well when using TV regularization. Because TV is not suitable in which the local structure has a dominant direction, the same situation will appear in Model 4, corresponding to the point of the stratum extinction zone.

The DTV regularization introduces the seismic dip attribute to project the data from the Cartesian coordinate system to the directions along and perpendicular to the seismic dip and then implements the differential operation. An illustration of the DTV regularization is shown in Fig. 1(b) with the dashed blue arrows.

Thus, (21) can be rewritten as

$$J_{\text{dtv}}(\mathbf{m}) = J(\mathbf{m}) + \alpha(||\nabla_1 \mathbf{m}||_1 + ||\nabla_2 \mathbf{m}||_1) \tag{22}$$

where ∇_1 and ∇_2 represent the gradient operators along and perpendicular to the dominant direction of the seismic dip. Once the seismic slope is obtained, ∇_1 and ∇_2 can be mapped to x- and y-coordinates as

$$\begin{pmatrix} \nabla_1 \mathbf{m}(i, j) \\ \nabla_2 \mathbf{m}(i, j) \end{pmatrix} = \Lambda \mathbf{R} \begin{pmatrix} \nabla_x \mathbf{m}(i, j) \\ \nabla_y \mathbf{m}(i, j) \end{pmatrix} \tag{23}$$

where the scaling matrix Λ and the rotation matrix $\mathbf{R}$ can be expressed as

$$\Lambda = \begin{pmatrix} \alpha_1 & 0 \\ 0 & \alpha_2 \end{pmatrix}, \quad \mathbf{R} = \begin{pmatrix} \cos\theta & -\sin\theta \\ \sin\theta & \cos\theta \end{pmatrix} \tag{24}$$

where α_1 and α_2 represent the scale on the gradient along and perpendicular to the seismic local dip θ.

The objective function, such as (20), can be solved by the split-Bregman algorithm. The algorithm can be seen in Algorithm 1. It means that there are two steps in each iteration time. First, the AVA inversion is done one by one in common reflection points (CRP) seismic data to obtain 2-D inversion results. Then, apply the DTV regularization to improve the inversion results.

III. NUMERICAL EXAMPLES

Here, we take the Society of Exploration Geophysicists (SEG)/European Association of Geoscientists and Engineers (EAGE) Marmousi model as an example to verify the effectiveness and superiority of the proposed strategy. V_p, V_s, and ρ models in the time domain can be seen in Fig. 2. The geological structure of this model is relatively sophisticated, including

This article has been accepted for inclusion in a future issue of this journal. Content is final as presented, with the exception of pagination.

HUANG *et al.*: DTV REGULARIZED HIGH-RESOLUTION PRESTACK AVA INVERSION

5

Algorithm 1 DTV Regularized High-Resolution Prestack Inversion

Input: initial model, seismic data

Output: high-resolution inversion results

1. **Executing** seismic migration process to obtain the post-stack or seismic images.

2. **Extracting** seismic slope from seismic data or images of Step 1 with PWD algorithm

3. **Initializing:** $\mathbf{m}^0 = \hat{\mathbf{m}}$, and $\mathbf{a}_1^0 = \mathbf{a}_2^0 = \mathbf{b}_1^0 = \mathbf{b}_2^0 = \mathbf{0}$.

4. **do while**(iter≤Maxiter or misfit≤ ϵ)

$$\mathbf{m}^{k+1} = \arg\min\left\{[\mathbf{d}-\mathbf{G}(\mathbf{m}^k)]^T[\mathbf{d}-\mathbf{G}(\mathbf{m}^k)]+(\mathbf{m}^k)^T\mathbf{C}_m(\mathbf{m}^k)\right\}$$

$$\mathbf{m}^{k+1} = \mathbf{m}^{k+1} - \lambda(\nabla_1^T(\mathbf{a}_1^k - \nabla_1\mathbf{m}^k - \mathbf{b}_1^k)$$
$$+ \nabla_2^T(\mathbf{a}_2^k - \nabla_2\mathbf{m}^k - \mathbf{b}_2^k)$$

$$\mathbf{a}_1^{k+1} = \text{shrink}(\nabla_1\mathbf{m}^{k+1} + \mathbf{b}_1^k, (1/\lambda))$$

$$\mathbf{b}_1^{k+1} = \mathbf{b}_1^k + (\nabla_1\mathbf{m}^{k+1} - \mathbf{a}_1^{k+1})$$

$$\mathbf{a}_2^{k+1} = \text{shrink}(\nabla_2\mathbf{m}^{k+1} + \mathbf{b}_2^k, (1/\lambda))$$

$$\mathbf{b}_2^{k+1} = \mathbf{b}_2^k + (\nabla_2\mathbf{m}^{k+1} - \mathbf{a}_2^{k+1})$$

where $\text{shrink}(m, \rho) = (m/|m|) * \max(|m| - \rho, 0)$.

end

5. Output the inversion result $\mathbf{m}_{k+1}$ and starting model $\hat{\mathbf{m}}$
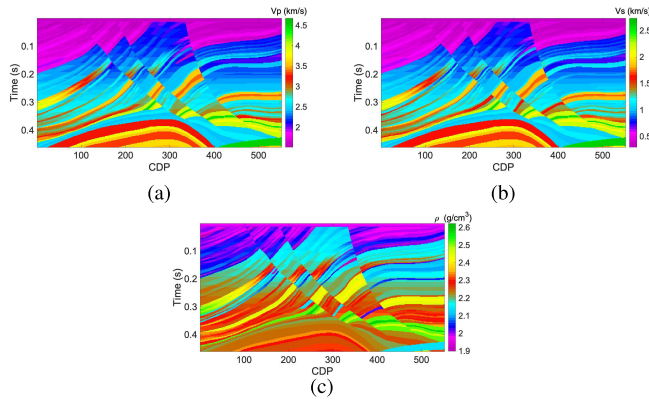

Fig. 2.　(a) v_p, (b) v_s, and (c) ρ parameters of the partial Marmousi model.

many tilted formations, faults, and other complex-textured geological structures.

With the elastic parameters, the reflection coefficient can be obtained using (1). Then, convolving the reflectivities with a zero-phase 30-Hz Ricker wavelet, we obtain a zero-offset synthetic seismic profile, as shown in Fig. 3(a). As a key factor of this method, the seismic slope angle can be extracted from the poststack seismic data. Fig. 3(b) shows the extracted seismic slope attribute by using PWD. The estimated slope provides us with the key to rotate the coordinate system when using the proposed DTV regularization.

Then, we applied the conventional ℓ_2-norm regularized method, the TV regularized method, and the DTV regularized method to the exact Zoeppritz AVA inversion, respectively.
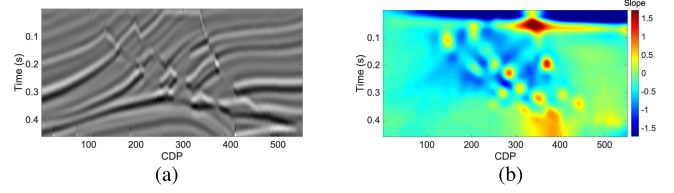

Fig. 3.　(a) Zero-offset synthetic data profile and (b) estimated seismic slope by using the PWD algorithm.

Figs. 7(a), 8(a), and 9(a) show the initial model, built by smoothing the model V_p, V_s, and ρ, for the AVA inversion. Here, we use a moving average filter to generate the starting model, and the span of the filter is ten samples. In order to obtain the low-frequency model, we smoothed the model five times in the horizontal and vertical directions, respectively. Because we use the gradient method to solve the inverse problem, a relative accurate model is very important for the inversion. Thus, we use a relatively accurate model as the initial model. The multiparameter inversion results are shown in Figs. 4–6, and we can observe the following phenomena.

Fig. 4 shows the starting model and inverted results (a) of the V_p parameters by using the ℓ_2-norm regularized method (b), the conventional TV regularized method (c), and the proposed DTV regularized method (d). It can be found that the smooth constraint (ℓ_2-norm regularization) leads to poor results describe the boundary. Although such a method can already restore the structure of the underground medium to a certain extent, it is not ideal for the detailed description. The geological structures and interfaces are blurred, and the ability to describe the fault is even worse.

Compared with the ℓ_2-norm regularization, the TV regularization improves the ability of the inversion method to describe the boundary, as shown in Fig. 4(c). Besides, the TV regularization better resolves some defects of the conventional trace-alone method. Especially at locations where the seismic slope is small, both the vertical and horizontal resolutions of the inversion results have been improved. However, when the stratum is tilted severely, even when a fault occurs, the method has a discontinuity in the horizontal direction. In this case, the difference in the traditional Cartesian coordinate system is likely to cause anomalies due to the drastic lateral change of parameters. The main problem is that there are many vertical artifacts in the results on the profiles of the inversion results.

Further comparing the inverted results using the proposed method and the former two, the latter one improves the inverted results by avoiding the artifacts in the inverted results, as shown in Fig. 4(d). Besides, the interface, tilted strata, and faults have been very well characterized, and the details have been greatly improved. The essence of TV regularization is to highlight the sparsity of the first-order difference, that is, to make use of the characteristics of discontinuous interface information to highlight anomalies. When the interface is tilted, DTV can rotate the coordinate system according to the slope information to highlight this abnormality to the greatest extent. It is obvious that it is a very creative design, which makes the tilted interface better portrayed.
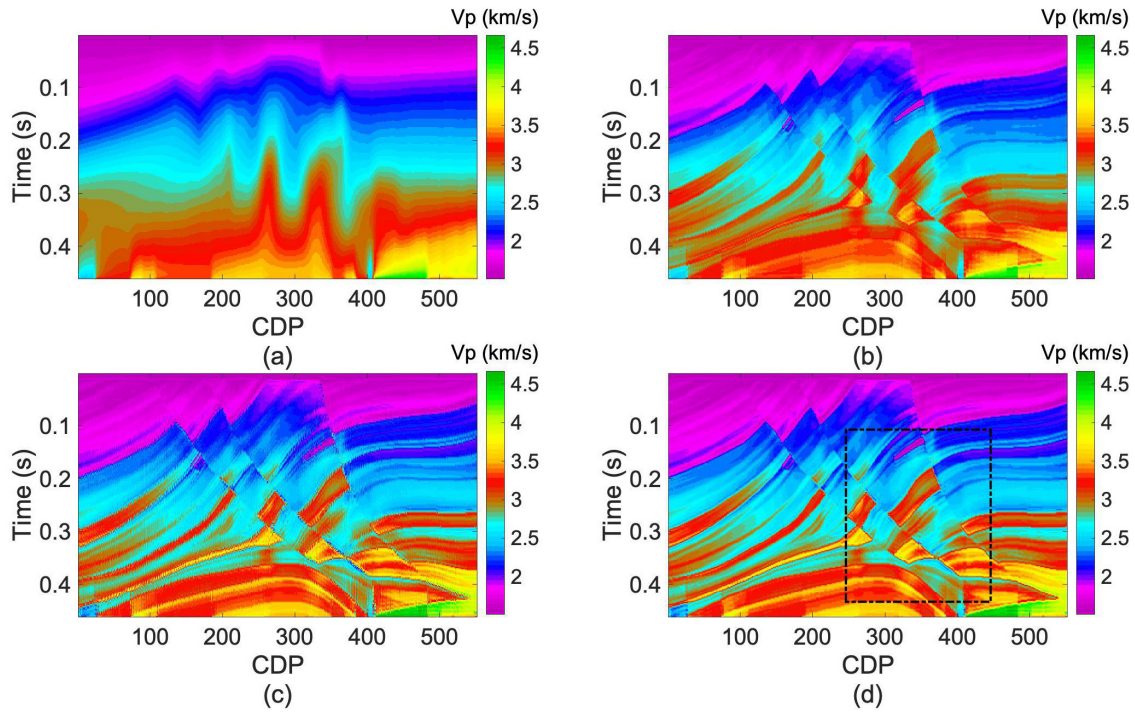
Fig. 4.   (a) Starting model and inverted results of the V_p parameters by using (b) ℓ_2-norm regularized method, (c) conventional TV regularized method, and (d) proposed DTV regularized method.
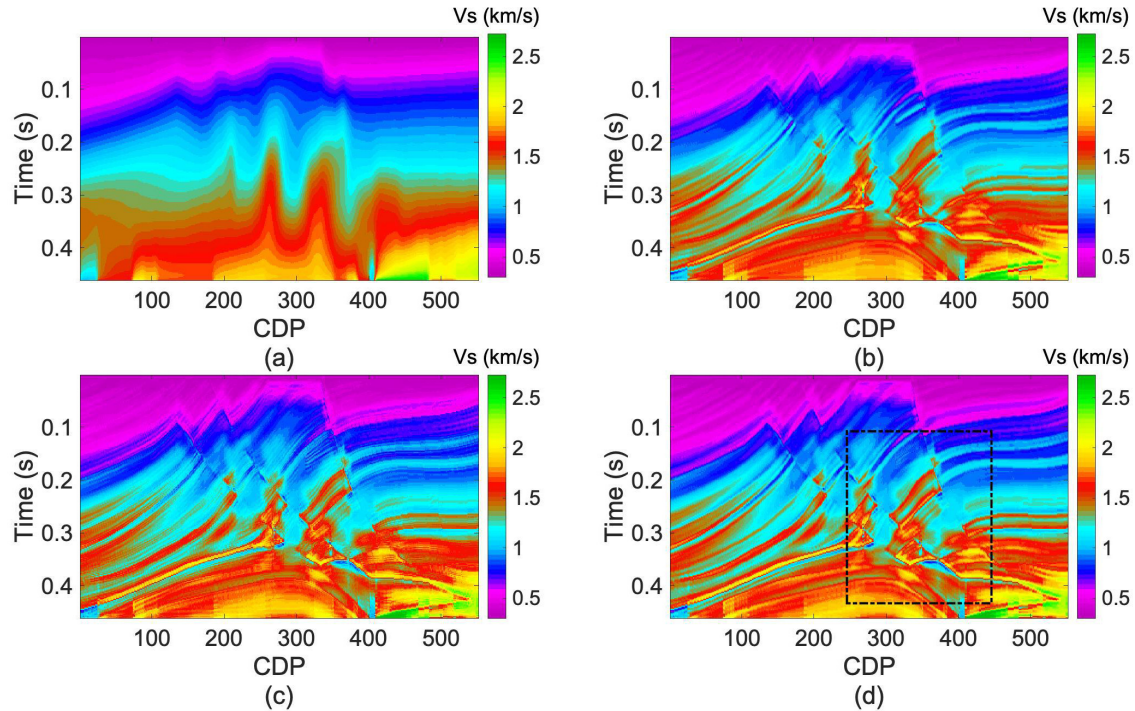

Fig. 5.   (a) Starting model and inverted results of the Vs parameters by using (b) ℓ_2-norm regularized method, (c) conventional TV regularized method, and (d) proposed DTV regularized method.

To further verify the superiority of the proposed method, we magnified the most violent part of the strata, which corresponds to the black dotted rectangle in Figs. 4(d), 5(d), and 6(d). The extracted results are shown in Figs. 7–9. The results are consistent with the previous conclusions but are much clearer. Compared with V_p and ρ, the results of V_s are slightly worse. This is because the P-P wave seismic data are not sensitive to V_s. Further improving the V_s inversion result is the future research direction.
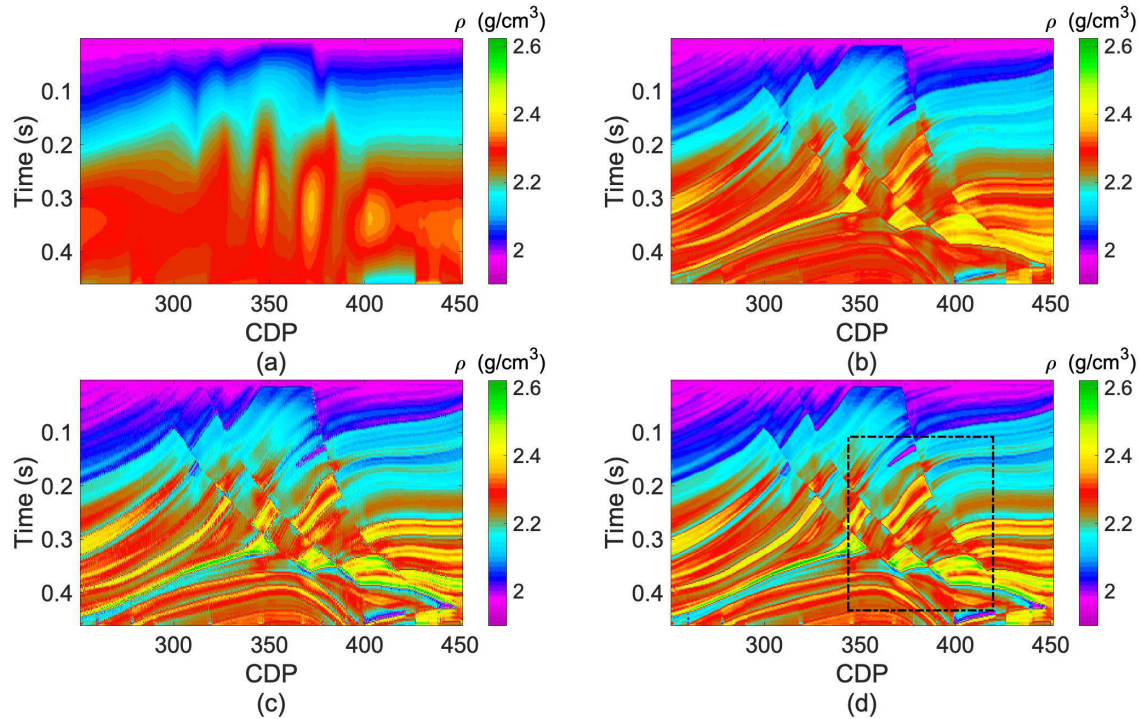
This article has been accepted for inclusion in a future issue of this journal. Content is final as presented, with the exception of pagination.

HUANG *et al.*: DTV REGULARIZED HIGH-RESOLUTION PRESTACK AVA INVERSION

7

Fig. 6. (a) Starting model and inverted results of the ρ parameters by using (b) ℓ_2-norm regularized method, (c) conventional TV regularized method, and (d) proposed DTV regularized method.
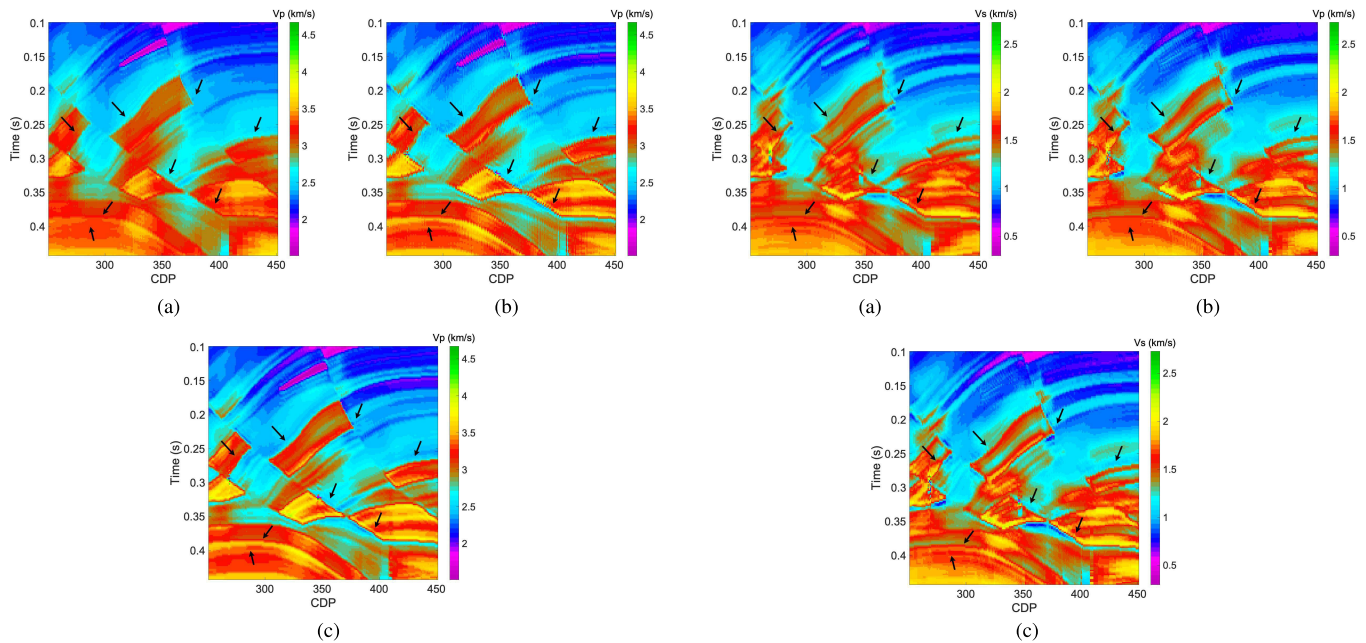

Fig. 7. Partially zoomed inverted V_p by using (a) ℓ_2-norm regularized method, (b) conventional TV regularized method, and (c) proposed DTV regularized method.
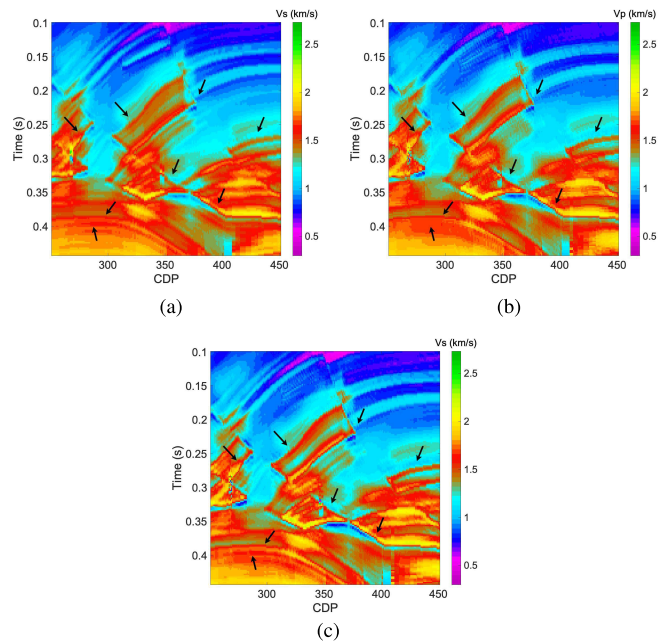

Fig. 8. Partially zoomed inverted Vs by using (a) ℓ_2-norm regularized method, (b) conventional TV regularized method, and (c) proposed DTV regularized method.

Then, to further verify the anti-noise property of the proposed method, a full-band Gaussian random noise is added to the observed data, and then, it yields the noise corrupted seismic data with SNR of 3 and 1, respectively. We inverted the elastic parameters by using the proposed method, the zoomed-inverted P-wave velocity profiles can be

seen in Fig. 10. We can find that TV regularization itself is an image processing method; we can still get a very good inversion result by using the noise corrupted seismic data. However, compared with Fig. 9(c), it can be found that the image result is, indeed, affected by a certain amount of noise.
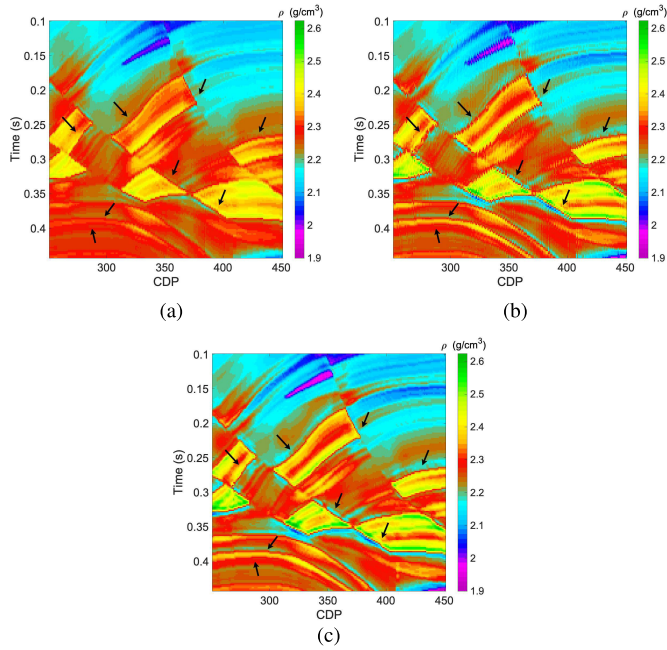
Fig. 9. Partially zoomed inverted ρ by using (a) ℓ_2-norm regularized method, (b) conventional TV regularized method, and (c) proposed DTV regularized method.
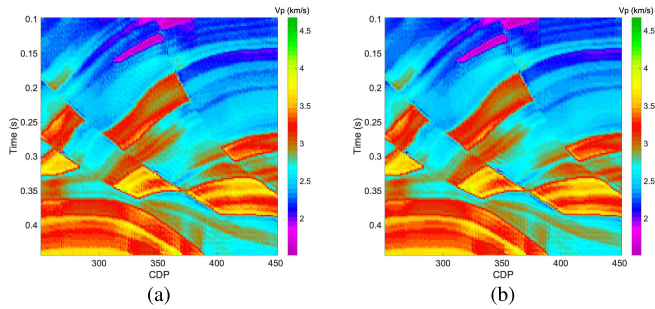

Fig. 10. Inverted result by using the DTV regularization with noise corrupted seismic data; the SNRs are (a) 3 and (b) 1.
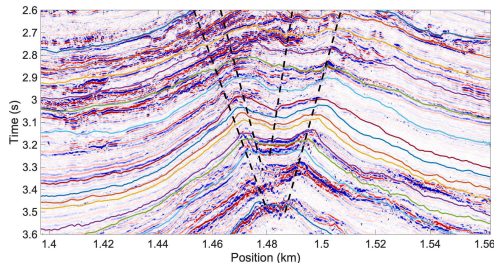

Fig. 11. Poststack seismic profile of the real seismic data and the artificial interpretation.

IV. REAL DATA APPLICATION

To further verify the superiority and universality of the proposed method, we applied a set of real seismic data for inversion, which comes from the Galio oilfield, Angola. The hydrocarbon mainly accumulates in the Lower Congo Basin and the Kwanza Basin. The total sedimental system includes both subsalt and postsalt source rocks and Oligocene to Miocene turbidite reservoirs.
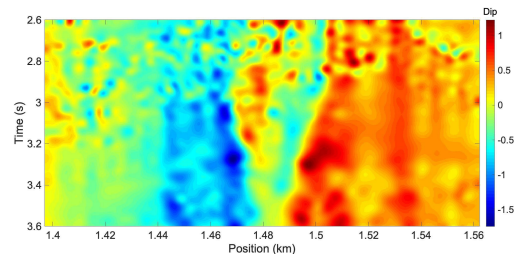

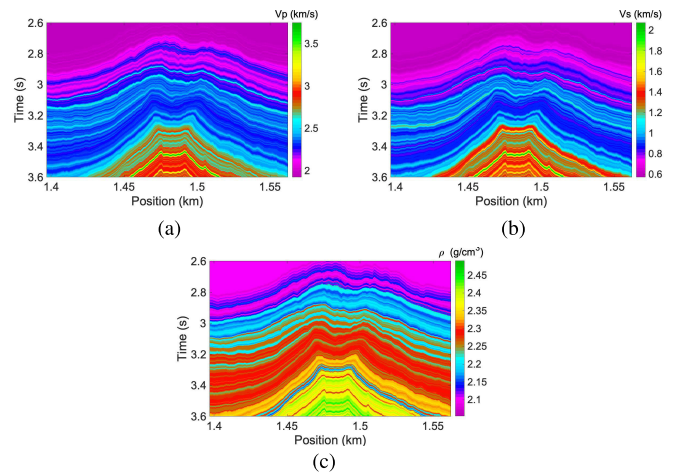Fig. 12. Estimated slope of the seismic data by using the PWD algorithm.

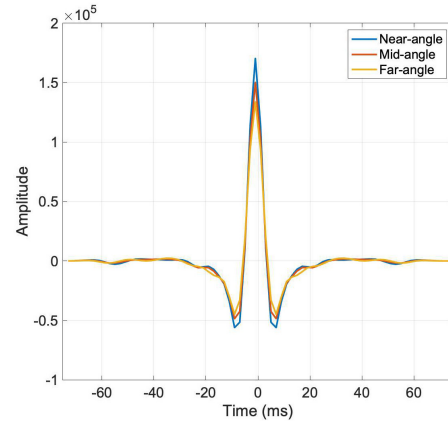Fig. 13. Starting model of (a) v_p, (b) v_s, and (c) ρ for seismic inversion.

Fig. 14. Near-, mid-, and far-angle seismic wavelets extracted from the prestack angle gather.

Fig. 11 shows the poststack seismic profile. It can be found that the subsurface medium structure in this area is complex, and the seismic signal-to-noise ratio is low. Therefore, it is very difficult to carry out horizon interpretation and fault interpretation of such data, and it is easy to cause manual interpretation errors. However, in order to provide a more accurate starting model for the seismic inversion, we spent a lot of energy interpreting the geological horizons. The figure shows the interpretation results of 13 horizons (solid color line) and four dominant faults (black dashed lines). Then, we extract the seismic slope attribute from the poststack seismic data by using the PWD algorithm for the proposed
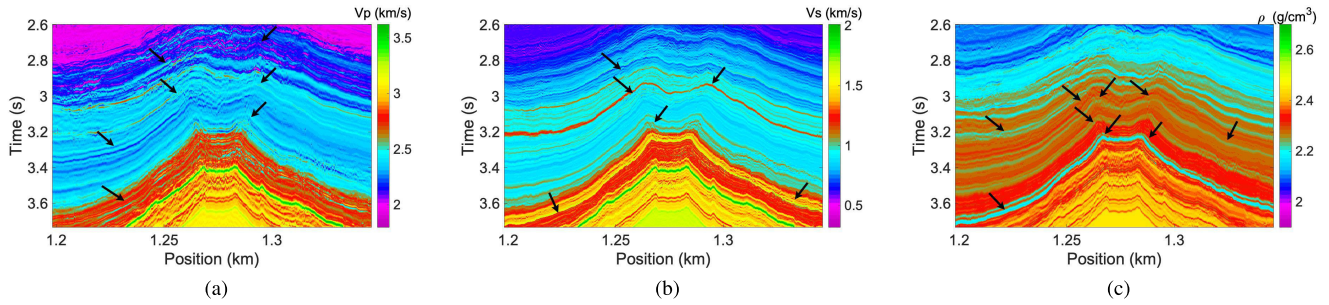
Fig. 15. Real seismic data inversion results (a) V_p, (b) V_s, and (c) ρ by using the ℓ_2-norm regularization.
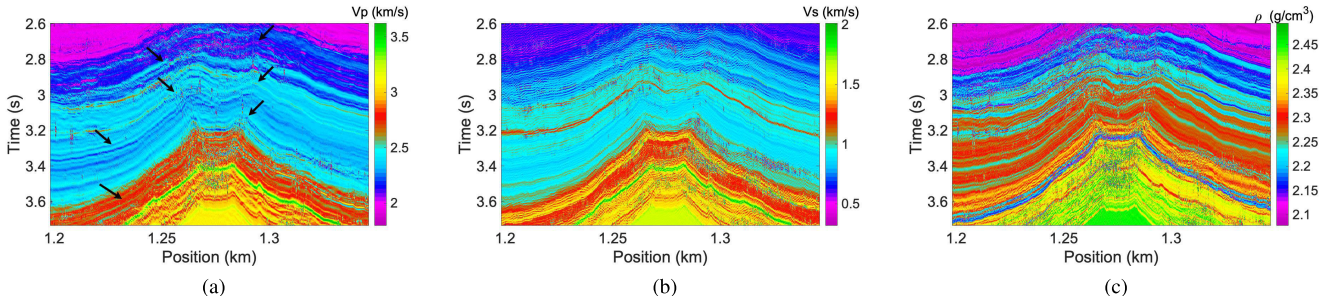

Fig. 16. Real seismic data inversion results (a) V_p, (b) V_s, and (c) ρ by using the conventional TV regularization.
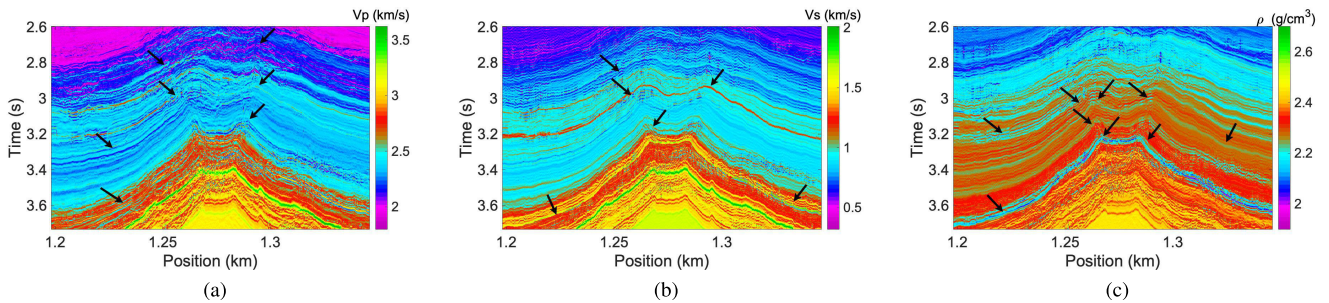

Fig. 17. Real seismic data inversion results (a) V_p, (b) V_s, and (c) ρ by using the proposed DTV regularization.

method, as shown in Fig. 12. Then, we use the results of geological horizon interpretation and well-logs to build the initial model, as shown in Fig. 13 [59].

For prestack AVA inversion, seismic wavelets are another significant factor for seismic inversion. We extract the seismic wavelet from the prestack seismic data, as shown in Fig. 13. Then, we exploit the exact Zoeppritz equation as a forward operator for the inversion. The ℓ_2-norm, the conventional TV norm, and the proposed DTV norm are the penalty norms for the prestack inversion. Figs. 15–17 show the inversion results corresponding to their inversion results.

Fig. 15 indicates the obtained V_p, V_s, and ρ results by using the ℓ_2-norm as a penalty. It can be seen that the result is too smooth, the formation interface is blurred, and it is almost impossible to distinguish the position of the formation interface. Besides, due to the low signal-to-noise ratio of the seismic data, the inversion results have a problem of poor horizontal continuity, indicating that the traditional method has the disadvantage of poor stability.

Fig. 16 denotes the inversion results by using conventional TV regularization. Compared with the former, the quality of

these results has been improved, and the vertical resolution has been enhanced. However, due to the tilted layers and steep faults, the conventional TV regularization method still does not solve the problem of poor vertical and horizontal resolution very well. In particular, when there is a serious inclination of the stratum, a staircase effect will appear in the final inversion profile.

Fig. 17 corresponds to the inverted V_p, V_s, and ρ parameters by using the proposed method. Compared with the other two methods, we can find that the quality of the inversion results has been significantly improved. As shown in Figs. 14 and 15, we can clearly see the information of the formation interface, the position of the reflection interface of the formation, and the occurrence of the tilted structures, even for the steep fault. Besides, the lateral continuity is delineated well, showing the strong robustness of the proposed method. However, we can find that, when the faults are developed seriously, especially when the faults are staggered, the slope estimation could be inaccurately estimated. In this case, there will still be a staircase effect on the proposed DTV. In addition, noise interruption is also a disturbing factor for slope estimation. Thus,

it is very important to investigate more advanced algorithms for improving the quality of the seismic data.

V. CONCLUSION

TV regularization describes the spatial variation boundary of data by highlighting the sparsity of the first-order difference, which is regarded as an effective technical means for improving the resolution of blurred inversion results. However, due to the nongrid directional variations of the subsurface properties, conventional TV regularization always suffer from the staircase effect. In this article, we innovatively incorporate seismic dip attributes into TV regularization for the prestack inversion algorithm. By rotating the coordinate system according to the seismic slope, the proposed method can alleviate the staircase effect, while preserving the details, and further improve the resolution and lateral continuity of the inversion results. The inversion results of the synthetic data and real seismic data demonstrate that the superiority of the proposed method. Taking advantage of the DTV regularization algorithm, the proposed method inverted the subsurface properties with better resolution (in both horizontal and vertical directions) and robustness. Especially, in the presence of complex geological structures, the DTV regularization method shows more obvious advantages.

REFERENCES

[1] S. Karimpouli and A. Malehmir, "Neuro-Bayesian facies inversion of prestack seismic data from a carbonate reservoir in Iran," *J. Petroleum Sci. Eng.*, vol. 131, pp. 11–17, Jul. 2015.

[2] K. Li, X.-Y. Yin, and Z.-Y. Zong, "Pre-stack Bayesian cascade AVA inversion in complex-laplace domain and its application to the broadband data acquired at east China," *J. Petroleum Sci. Eng.*, vol. 158, pp. 751–765, Sep. 2017.

[3] Q. Liu, N. Dong, Y. Ji, and T. Chen, "Direct reservoir property estimation based on prestack seismic inversion," *J. Petroleum Sci. Eng.*, vol. 171, pp. 1475–1486, Dec. 2018.

[4] G. Cheng, X. Yin, and Z. Zong, "Nonlinear elastic impedance inversion in the complex frequency domain based on an exact reflection coefficient," *J. Petroleum Sci. Eng.*, vol. 178, pp. 97–105, Jul. 2019.

[5] X. Pan, G. Zhang, and Y. Cui, "Matrix-fluid-fracture decoupled-based elastic impedance variation with angle and azimuth inversion for fluid modulus and fracture weaknesses," *J. Petroleum Sci. Eng.*, vol. 189, Jun. 2020, Art. no. 106974.

[6] G. Huang, X. Chen, J. Li, C. Luo, and B. Wang, "Application of an adaptive acquisition regularization parameter based on an improved GCV criterion in pre-stack AVO inversion," *J. Geophys. Eng.*, vol. 14, no. 1, pp. 100–112, Jan. 2017.

[7] Q. Guo, H. Zhang, F. Han, and Z. Shang, "Prestack seismic inversion based on anisotropic Markov random field," *IEEE Trans. Geosci. Remote Sens.*, vol. 56, no. 2, pp. 1069–1079, Feb. 2018.

[8] G. Huang, X. Chen, C. Luo, and X. Li, "Application of optimal transport to exact Zoeppritz equation AVA inversion," *IEEE Geosci. Remote Sens. Lett.*, vol. 15, no. 9, pp. 1337–1441, Jun. 2018.

[9] Q. Guo, H. Zhang, K. Wei, Z. Li, and Z. Shang, "An improved anisotropic Markov random field approach for prestack seismic inversion," *IEEE Geosci. Remote Sens. Lett.*, vol. 16, no. 4, pp. 633–637, Apr. 2019.

[10] Q. Guo, H. Zhang, H. Cao, W. Xiao, and F. Han, "Hybrid seismic inversion based on multi-order anisotropic Markov random field," *IEEE Trans. Geosci. Remote Sens.*, vol. 58, no. 1, pp. 407–420, Jan. 2020.

[11] C. Luo, X. Li, and G. Huang, "Pre-stack AVA inversion by using propagator matrix forward modeling," *Pure Appl. Geophys.*, vol. 176, no. 10, pp. 4445–4476, Oct. 2019.

[12] L. Zhi, S. Chen, and X. Li, "Amplitude variation with angle inversion using the exact Zoeppritz equations—Theory and methodology," *Geophysics*, vol. 81, no. 2, pp. N1–N15, 2016.

[13] G. Huang, J. Li, C. Luo, and X. Chen, "Regularization parameter adaptive selection and its application in the pre-stack AVO inversion," *Explor. Geophys.*, vol. 49, no. 3, pp. 323–335, 2018.

[14] J. P. Castagna and S. W. Smith, "Comparison of AVO indicators: A modeling study," *Geophysics*, vol. 59, no. 12, pp. 1849–1855, Dec. 1994.

[15] Z. Zong, X. Yin, and G. Wu, "Multi-parameter nonlinear inversion with exact reflection coefficient equation," *J. Appl. Geophys.*, vol. 98, pp. 21–32, Nov. 2013.

[16] F. Zhang, R. Dai, and H. Liu, "High order approximation for scattering matrix in layered elastic medium and its application in pre-stack seismic inversion," *J. Petroleum Sci. Eng.*, vol. 131, pp. 210–217, Jul. 2015.

[17] A. Tarantola, *Inverse Problem Theory and Methods for Model Parameter Estimation*. Philadelphia, PA, USA: SIAM , 2005, vol. 89.

[18] D. R. Velis, "Constrained inversion of reflection data using Gibbs' sampling," *J. Seismic Explor.*, vol. 14, no. 1, p. 31, 2005.

[19] D. O. Pérez, D. R. Velis, and M. D. Sacchi, "Three-term inversion of prestack seismic data using a weighted L2, 1 mixed norm," *Geophys. Prospecting*, vol. 65, no. 6, pp. 1477–1495, 2017.

[20] C. Li and F. Zhang, "Amplitude-versus-angle inversion based on the L_1-norm-based likelihood function and the total variation regularization constraint," *Geophysics*, vol. 82, no. 3, pp. R173–R182, 2017.

[21] A. Buland and H. Omre, "Bayesian linearized AVO inversion," *Geophysics*, vol. 68, no. 1, pp. 185–198, Jan. 2003.

[22] T. Erik Rabben, H. Tjelmeland, and B. Ursin, "Non-linear Bayesian joint inversion of seismic reflection coefficients," *Geophys. J. Int.*, vol. 173, no. 1, pp. 265–280, Apr. 2008.

[23] S. Geman and D. Geman, "Stochastic relaxation, Gibbs distributions, and the Bayesian restoration of images," *IEEE Trans. Pattern Anal. Mach. Intell.*, vol. PAMI-6, no. 6, pp. 721–741, Nov. 1984.

[24] D. Geman and G. Reynolds, "Constrained restoration and the recovery of discontinuities," *IEEE Trans. Pattern Anal. Mach. Intell.*, vol. 14, no. 3, pp. 367–383, Mar. 1992.

[25] D. Geman and C. Yang, "Nonlinear image recovery with half-quadratic regularization," *IEEE Trans. Image Process.*, vol. 4, no. 7, pp. 932–946, Jul. 1995.

[26] P. Charbonnier, L. Blanc-Feraud, G. Aubert, and M. Barlaud, "Deterministic edge-preserving regularization in computed imaging," *IEEE Trans. Image Process.*, vol. 6, no. 2, pp. 298–311, Feb. 1997.

[27] J. S. Bhatt and M. V. Joshi, *Regularization Hyperspectral Unmixing*. Bellingham, WA, USA: SPIE, 2016.

[28] D. Terzopoulos, "Regularization of inverse visual problems involving discontinuities," *IEEE Trans. Pattern Anal. Mach. Intell.*, vol. PAMI-8, no. 4, pp. 413–424, Jul. 1986.

[29] W. Alemie and M. D. Sacchi, "High-resolution three-term AVO inversion by means of a trivariate cauchy probability distribution," *Geophysics*, vol. 76, no. 3, pp. R43–R55, May 2011.

[30] R. Zhang and J. Castagna, "Seismic sparse-layer reflectivity inversion using basis pursuit decomposition," *Geophysics*, vol. 76, no. 6, pp. R147–R158, Nov. 2011.

[31] R. Zhang, M. K. Sen, and S. Srinivasan, "A prestack basis pursuit seismic inversion," *Geophysics*, vol. 78, no. 1, pp. R1–R11, Jan. 2013.

[32] H. Zhang, Z. Shang, and C. Yang, "A non-linear regularized constrained impedance inversion," *Geophys. Prospecting*, vol. 55, no. 6, pp. 819–833, Nov. 2007.

[33] L. Liang, H. Zhang, Q. Guo, W. Saeed, Z. Shang, and G. Huang, "Stability study of pre-stack seismic inversion based on the full zoeppritz equation," *J. Geophys. Eng.*, vol. 14, no. 5, pp. 1242–1259, Oct. 2017.

[34] Y.-K. Tian, H. Zhou, H.-M. Chen, Y.-M. Zou, and S.-J. Guan, "Bayesian prestack seismic inversion with a self-adaptive huber-Markov random-field edge protection scheme," *Appl. Geophys.*, vol. 10, no. 4, pp. 453–460, Dec. 2013.

[35] K.-N. Wang, Z.-D. Sun, and N. Dong, "Prestack inversion based on anisotropic Markov random field–maximum posterior probability inversion and its application to identify shale gas sweet spots," *Appl. Geophys.*, vol. 12, no. 4, pp. 533–544, 2015.

[36] S. Qu and D. J. Verschuur, "Simultaneous time-lapse imaging via joint migration and inversion," in *Proc. 78th EAGE Conf. Exhibit.*, May 2016, pp. 1–5.

[37] H. Zhang, Q. Guo, L. Liang, C. Cao, and Z. Shang, "A nonlinear method for multiparameter inversion of pre-stack seismic data based on anisotropic Markov random field," *Geophys. Prospecting*, vol. 66, no. 3, pp. 461–477, Mar. 2018.

[38] A. Y. Anagaw and M. D. Sacchi, "Edge-preserving seismic imaging using the total variation method," *J. Geophys. Eng.*, vol. 9, no. 2, pp. 138–146, Apr. 2012.

[39] A. Gholami, "Nonlinear multichannel impedance inversion by total-variation regularization," *Geophysics*, vol. 80, no. 5, pp. R217–R224, Sep. 2015.

[40] I. Bayram and M. E. Kamasak, "A directional total variation," in *Proc. 20th Eur. Signal Process. Conf. (EUSIPCO)*, 2012, pp. 265–269.

[41] I. Bayram and M. E. Kamasak, "Directional total variation," *IEEE Signal Process. Lett.*, vol. 19, no. 12, pp. 781–784, Dec. 2012.

[42] X. Zhu, D. P. Sixta, and B. G. Angstman, "Tomostatics: Turning-ray tomography+ static corrections," *Lead. Edge*, vol. 11, no. 12, pp. 15–23, 1992.

[43] C. A. Zelt and P. J. Barton, "Three-dimensional seismic refraction tomography: A comparison of two methods applied to data from the faeroe basin," *J. Geophys. Res.: Solid Earth*, vol. 103, no. B4, pp. 7187–7210, Apr. 1998.

[44] J. Korenaga *et al.*, "Crustal structure of the southeast greenland margin from joint refraction and reflection seismic tomography," *J. Geophys. Res.: Solid Earth*, vol. 105, no. B9, pp. 21591–21614, Sep. 2000.

[45] K. Osypov, "Robust refraction tomography," in *Proc. SEG Tech. Program Expanded Abstr.*, Jan. 2000, pp. 2032–2035.

[46] M. Noble, P. Thierry, C. Taillandier, and H. Calandra, "High-performance 3D first-arrival traveltime tomography," *Lead. Edge*, vol. 29, no. 1, pp. 86–93, Jan. 2010.

[47] S. Li, "Wave-equation migration velocity analysis by non-stationary focusing," in *Proc. SEG Tech. Program Expanded Abstr.*, Aug. 2013, pp. 1110–1115.

[48] J. Chen, C. A. Zelt, and P. Jaiswal, "A case history: Application of frequency-dependent traveltime tomography and full waveform inversion to a known near-surface target," in *Proc. SEG Tech. Program Expanded Abstr.*, Aug. 2013, pp. 1743–1748.

[49] M. K. Sen and I. G. Roy, "Computation of differential seismograms and iteration adaptive regularization in prestack waveform inversion," *Geophysics*, vol. 68, no. 6, pp. 2026–2039, Nov. 2003.

[50] J. F. Claerbout, *Earth Soundings Analysis: Processing Versus Inversion*. London, U.K.: Blackwell Scientific Publications, 1992.

[51] S. Fomel, "Applications of plane-wave destruction filters," *Geophysics*, vol. 67, no. 6, pp. 1946–1960, 2002.

[52] S. Fomel, M. M. Backus, M. V. DeAngelo, P. E. Murray, and B. A. Hardage, "Multicomponent seismic data registration for subsurface characterization in the shallow gulf of Mexico," in *Proc. All Days*, May 2003, pp. 781–784.

[53] S. Fomel, M. Backus, K. Fouad, B. Hardage, and G. Winters, "A multistep approach to multicomponent seismic image registration with application to a West Texas carbonate reservoir study," in *Proc. SEG Tech. Program Expanded Abstr.*, Jan. 2005, pp. 1018–1021.

[54] Y. Chen, W. Huang, Y. Zhou, W. Liu, and D. Zhang, "Plane-wave orthogonal polynomial transform for amplitude-preserving noise attenuation," *Geophys. J. Int.*, vol. 214, no. 3, pp. 2207–2223, Sep. 2018.

[55] Y. Chen, H. Chen, K. Xiang, and X. Chen, "Preserving the discontinuities in least-squares reverse time migration of simultaneous-source data," *Geophysics*, vol. 82, no. 3, pp. S185–S196, May 2017.

[56] S. Qu, D. J. Verschuur, and Y. Chen, "Full waveform inversion using an automatic directional total variation constraint," in *Proc. 79th EAGE Conf. Exhib.*, Jun. 2017, pp. 1–5.

[57] S. Qu, E. Verschuur, and Y. Chen, "Full-waveform inversion and joint migration inversion with an automatic directional total variation constraint," *Geophysics*, vol. 84, no. 2, pp. R175–R183, Mar. 2019.

[58] J.-P. Thiran, "Recursive digital filters with maximally flat group delay," *IEEE Trans. Circuit Theory*, vol. 18, no. 6, pp. 659–664, Nov. 1971.

[59] G. Huang, X. Chen, C. Luo, and Y. Chen, "Geological structure-guided initial model building for prestack AVO/AVA inversion," *IEEE Trans. Geosci. Remote Sens.*, vol. 59, no. 2, pp. 1784–1793, Feb. 2021.

Xiaohong Chen received the B.S. degree in mathematics from Nanjing University, Nanjing, China, in 1982, the M.S. degree in applied mathematics from the Harbin Institute of Technology, Harbin, China, in 1988, and the Ph.D. degree in applied geophysics from the China University of Petroleum (Beijing) (CUPB), Beijing, China, in 1993.

In 1997, he was a Visiting Scholar with Columbia University, New York, NY, USA. He is a Professor of applied geophysics with CUPB. His research interests include signal processing, seismic inversion, and time-lapse seismic reservoir monitoring.
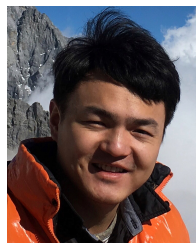
Shan Qu received the B.Sc. and M.Sc. degrees in geophysics from the China University of Petroleum (Beijing), Beijing, China, in 2012 and 2015, respectively. She is pursuing the Ph.D. degree with the Delphi Consortium, Delft University of Technology, Delft, The Netherlands. Her M.Sc. thesis topic was on the deblending of simultaneous source seismic data.

She holds a post-doctoral position at the Delphi Consortium, where she is working on time-lapse application and uncertainty estimation in joint migration inversion under the supervision of D. J. Verschuur.

Ms. Qu is also a member of SEG and EAGE.

Min Bai received the Ph.D. degree in geophysics from the China University of Petroleum (Beijing), Beijing, China, in 2016, under the supervision of Prof. Xiaohong Chen.

He is an Associate Professor with Yangtze University, Wuhan, China. He has published more than 30 journal articles. His research interests include seismic imaging and inversion, and seismic signal analysis.

Guangtan Huang received the B.S., M.S., and Ph.D. degrees in exploration geophysics from the China University of Petroleum (East China), Beijing, China, in 2012, 2015, and 2019, respectively.

From 2019 to 2021, he was a Post-Doctoral Research Associate with Zhejiang University, Hangzhou, China. He is an Assistant Researcher with the Institute of Rock and Soil Mechanics, Chinese Academy of Sciences, Wuhan, China. His research interests include seismic forward modeling and high-resolution seismic inversion.

Yangkang Chen (Member, IEEE) received the B.S. degree in exploration geophysics from the China University of Petroleum (Beijing), Beijing, China, in 2012, and the Ph.D. degree in geophysics from The University of Texas at Austin, Austin, TX, USA, in 2015, under the supervision of Prof. Sergey Fomel.

He was a Distinguished Post-Doctoral Research Associate with the Oak Ridge National Laboratory, Oak Ridge, TN, USA, where he conducted research on global adjoint tomography. He is an Assistant Professor with Zhejiang University, Hangzhou, China. He has authored or coauthored more than 100 internationally renowned journal articles and more than 80 international conference papers. His research interests include seismic signal analysis, seismic modeling and inversion, simultaneous-source data deblending and imaging, global adjoint tomography, machine learning, and high-performance computing.